Supplementary data

Nanomedicine-mediated co-expression of PD-1 blockade and CXCL9 synergizes T cell infiltration and activation in solid tumor

Yan Wang, ‡ * [a] Liang Zhao, ‡ [b] Jia-Yu Luo, ‡ [c] Jie Li, [a] Xin-Ya Gao, [a] Hui-Xiao Li, [d] Yue Zheng [a] and Jia-Wei Liu * [e]

a State Key Laboratory of Marine Environmental Science, and College of the Environment and Ecology, Xiamen University, Xiamen 361102, P. R. China.

b School of Food and Drug, Shenzhen Polytechnic university, Shenzhen 518055, P. R. China.

c Basic Medicine Teaching and Research Office, Zhuhai Health School, Zhuhai 519000, P. R. China.

d Center for Medical Genetics and Genomics, The Second Affiliated Hospital of Guangxi Medical University, Nanning 530007, P. R. China.

e Biogeomagnetism Lab, Key Laboratory of Planetary Science and Frontier Technology, Institute of Geology and Geophysics, Chinese Academy of Sciences, Beijing 100029, P. R. China.

‡ These authors contributed equally.

***Corresponding author:**

wangyanlq11@xmu.edu.cn (Yan Wang)

liujiawei@mail.iggcas.ac.cn (Jia-Wei Liu)

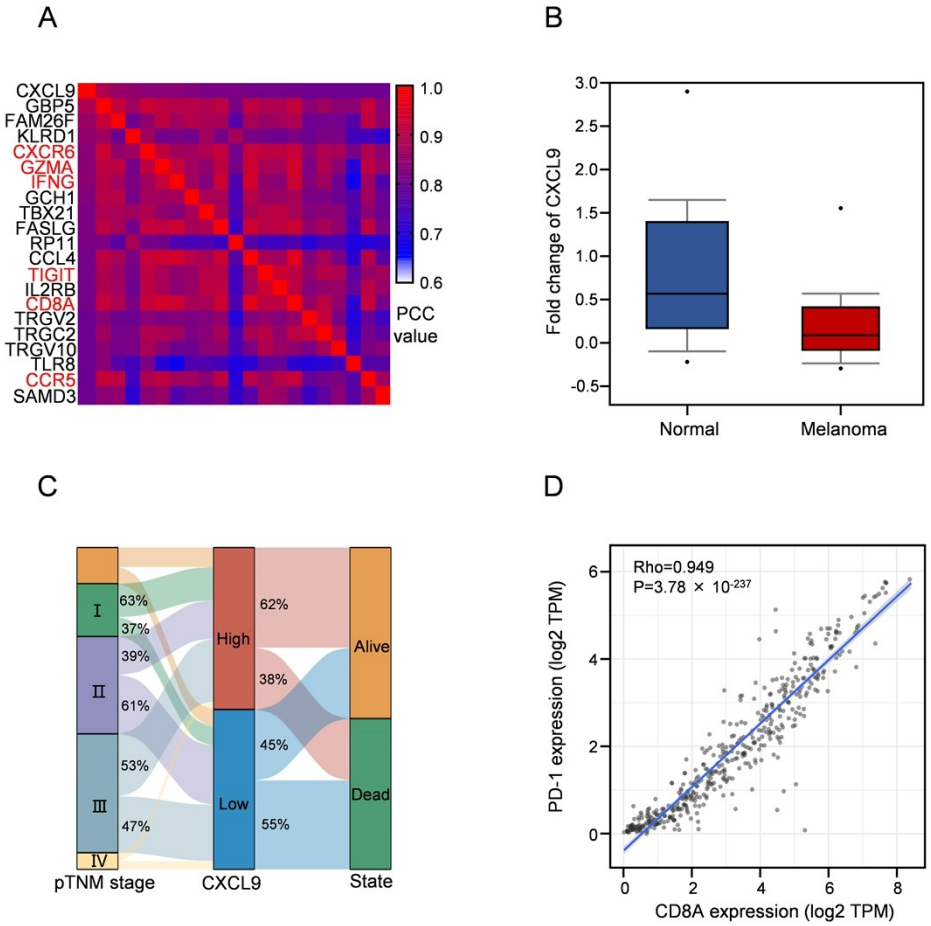

Fig. S1 (A) Heat map of twenty genes co-expressed with CXCL9 in melanoma. (B) Analyzing the fold change of CXCL9 in normal tissues and melanoma tissues using the data from TCGA database. (C) Sankey diagram for analyzing the percentage of melanoma patients in different parameters, the corresponding clinical information of patients was obtained from TCGA database. (D) Pearson correlation plot for the expression of CD8A and CXCL9 in skin cutaneous melanoma from TIMER website.

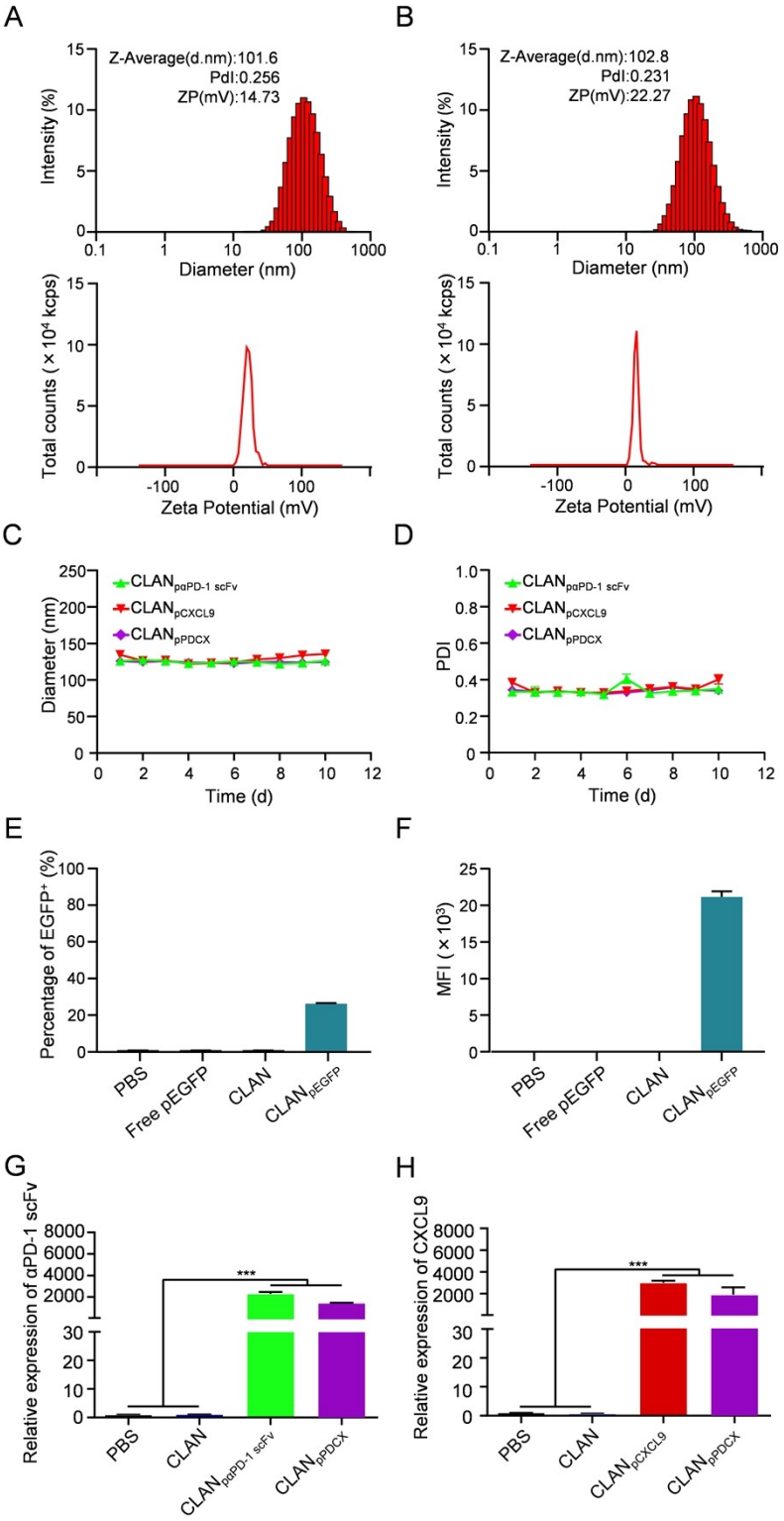

Fig. S2 (A, B) Size distributions and zeta potentials of $CLAN_{p\alpha PD\text{-}1\ scFv}$ and $CLAN_{pCXCL9}$. (C) and (D) The serum stability of particle size/PDI within 10% FBS. (E) and (F) Flow cytometry analysis of the percentage and mean fluorescence intensity (MFI) of EGFP-positive B16-F10 cells after transfection. (G, H) The mRNA levels of αPD-1 scFv and CXCL9 detected by qRT-PCR. Data are shown as the means ± SD (n = 3), one-way ANOVA with *post-hoc* analysis (G, H), *** $P < 0.001$.

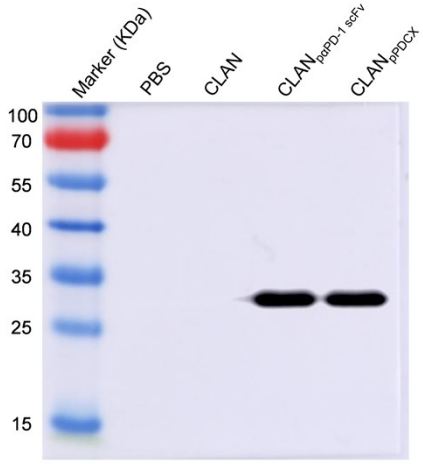

Fig. S3 Western blot for detecting the protein level of αPD-1 scFv using the mouse anti-6 × His tag antibody.

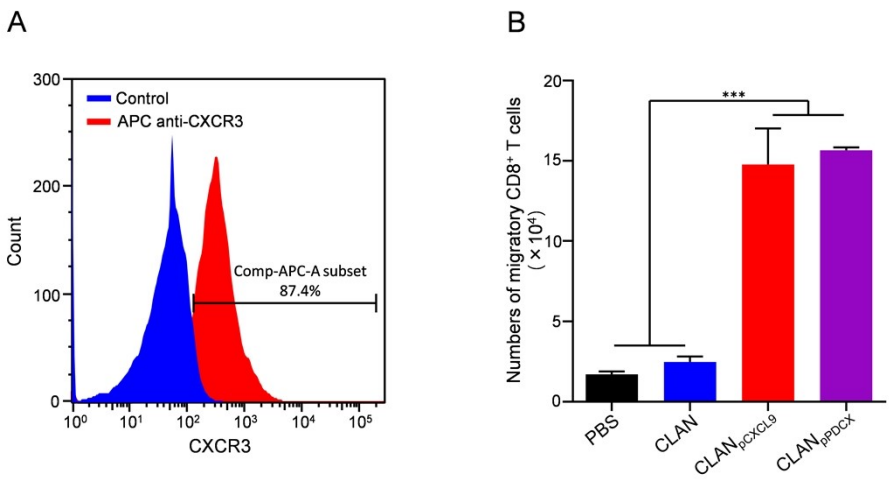

Fig. S4 (A) Flow cytometry for detecting the percentage of CXCR3-positive in $CD8^+$ T cells after 96 hours stimulation. (B) Quantitative analysis for the migration of $CD8^+$ T cells from the upper to the lower transwell chambers. Data are shown as the means ± SD (n = 3), one-way ANOVA with *post-hoc* analysis (C), *** $P < 0.001$.

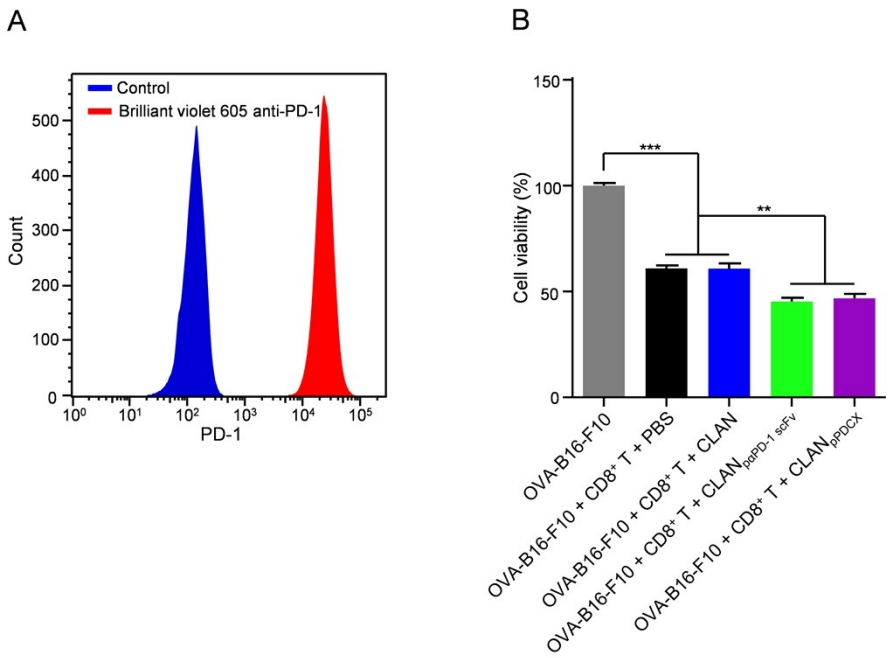

Fig. S5 (A) Flow cytometry for detecting the percentage of PD-1-positive mouse T lymphoma EL4 cells. (B) Detecting the viability of B16-F10-OVA cells co-cultured with OVA-specific $CD8^+$ T cells when the supernatant containing αPD-1 scFv or other control was added into the cultural medium. Data are shown as the means ± SD (n = 3), one-way ANOVA with *post-hoc* analysis (C), ** $P < 0.01$, *** $P < 0.001$.

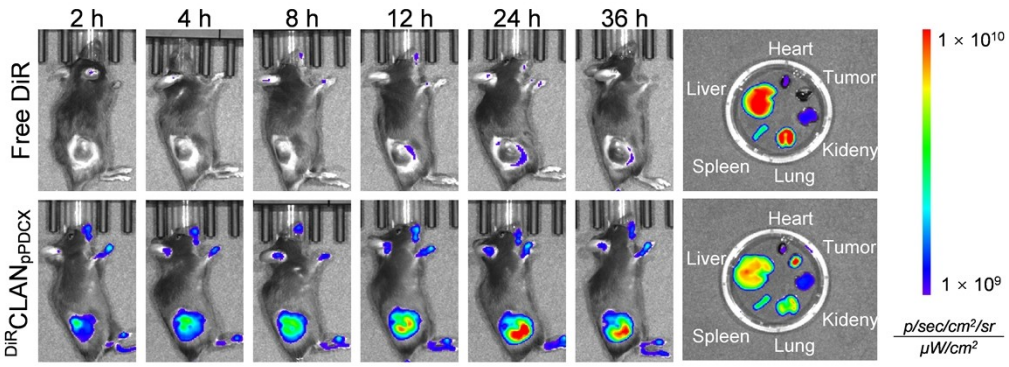

Fig. S6 The distribution of DiR-labeled $CLAN_{pPDCX}$ nanoparticles in B16-F10 melanoma-bearing mice. When the volume of subcutaneous B16-F10 melanoma reached 200-300 mm^3, the melanoma-bearing mice were intravenously injected with DiR-labeled $CLAN_{pPDCX}$. Two hours later, the fluorescent signal was detected and monitored until 36 h using the IVIS Spectrum (PerkinElmer, MA, USA).

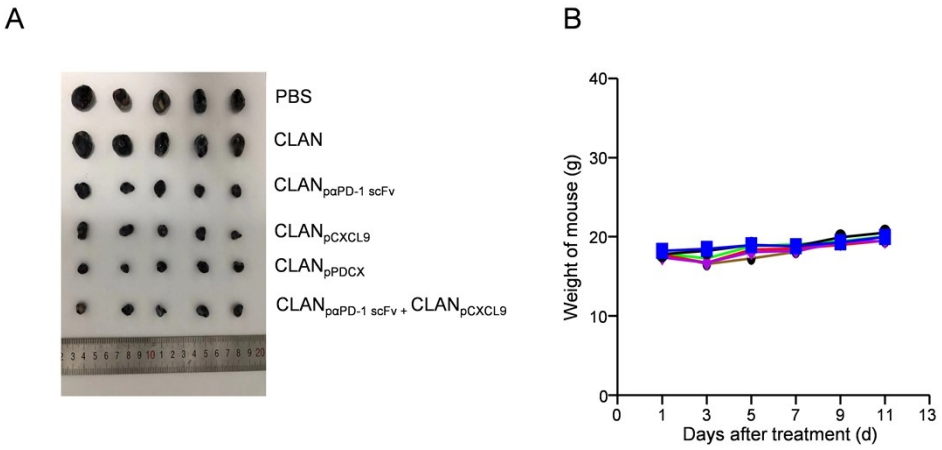

Fig. S7 (A) Tumor images of melanoma isolated from B16-F10-bearing mice at the end-point of the treatments. (B) Body weights of B16-F10-bearing mice during the treatments. Data are shown as the means ± SD (n = 5).

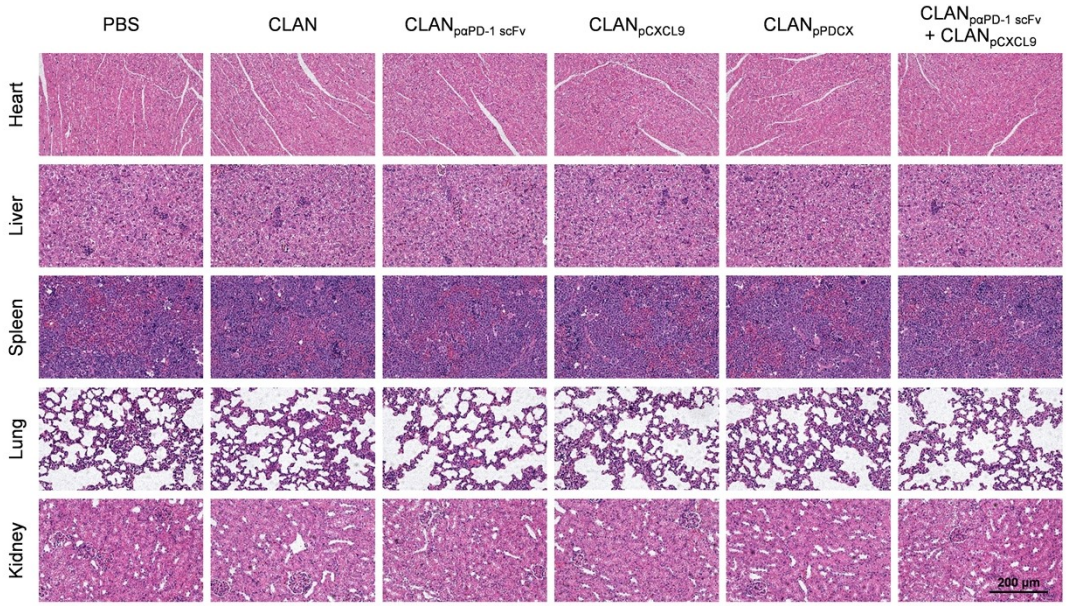

Fig. S8 H&E analysis of heart, liver, spleen, lung and kidney after the treatment of CLAN nanomedicines. The scale bar = 200 μm.

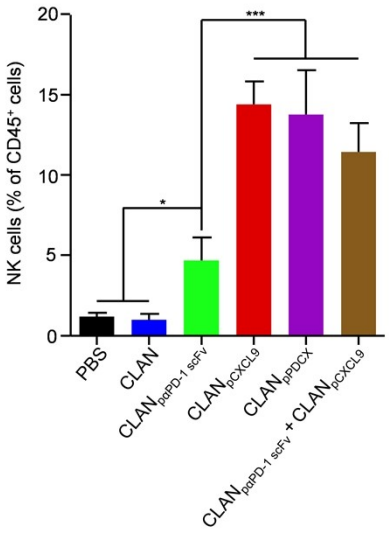

Fig. S9 Flow cytometry for analyzing the percentage of NK cells in tumor tissues at the end-point of the treatments. Data are shown as the means ± SD (n = 5), one-way ANOVA with *post-hoc* analysis, * $P < 0.05$, *** $P < 0.001$.